

Cite this: DOI: 00.0000/xxxxxxxxxx

Mechanical response of a simple DNA nanostar hydrogel: symptoms of disorder and glassy emergence of solidity.[†]Hajar Ajiyel,^{a,b,d} Anthony J. Genot,^{‡b} Soo Hyeon Kim,^b Nicolas Schabanel,^c Hervé Guillou,^a Catherine Barentin,^d and Mathieu Leocmach^{*d}Received Date
Accepted Date

DOI: 00.0000/xxxxxxxxxx

DNA self-assembly is a well-understood nanotechnology to obtain extremely ordered structures from the nanometer to up to the hundred of microns scale. By contrast, DNA hydrogels rely on the disordered assembly of DNA building blocks to reach macroscopic volumes. However, in order to hold the promise of DNA bulk materials, the sequence designer needs a systematic understanding of how macroscopic properties emerge from disorder. Here, we show a method to study systematically the mechanical response of a simple DNA nanostar hydrogel. This method mobilises bulk rheology, dynamic light scattering microrheology, mechanical modeling, as well as thermodynamic calculation and DNA sequence alteration. At low temperatures, we demonstrate a systematic deviation from Maxwell behaviour that is symptomatic of disordered materials. At temperatures much higher than the percolation of the DNA network, we characterise a surprising solid behaviour that we attribute to a glass transition. Our results show the importance of disorder in DNA materials. Furthermore, the method we showcase in this article can be widely applied to more complex DNA materials.

1 Introduction

In recent years, DNA has emerged as an ideal polymer to build soft materials. In addition to being mechanically robust, chemically stable and enzymatically replicable, DNA is a sequence-defined polymer. Two single-stranded DNA of complementary sequences can hybridize into the canonical double helix, forming a rigid bond. By smartly programming the monomer sequence, DNA can self-assemble into almost any shape¹. DNA nanostructures have been designed to dynamically respond to their chemical or mechanical environment by changing shape, disassembling, emitting light, etc.^{2,3}. Structures of hundreds of nanometers and hundreds of strands of complex shapes called ‘DNA origami’ are now routinely assembled (provided sufficient charge screening) from computer-aided design^{4,5} relying on the thermodynamics of DNA assembly to encode a geometry. Larger ordered structures can be produced⁶, up to hundreds of microns. However, such precise assemblies do not scale up well to bulk materials. To obtain centimeter-scale DNA materials, one has to embrace disorder and rely on the random assembly of DNA building blocks, sometimes associated to peptides, nanoparticles, synthetic poly-

mers, etc. These building blocks form a space-spanning network called a DNA hydrogel^{7,8}. Due to the disordered nature of DNA hydrogels, predicting their mechanical properties from the DNA sequence is a challenge.

In the present article, we focus on the simplest DNA hydrogel, and show how its mechanical properties can be characterized and understood down to the base pair level using methods from rheology, soft matter and statistical physics. In particular we demonstrate the fundamental role disorder at the nanoscale plays in the mechanical properties at the macroscale.

Our system belongs to the well-studied class of DNA nanostar hydrogels^{9–16}. It is composed solely of 3 strands of DNA that self-assemble into a 3-branch motif called a nanostar. Each arm ends in a palindromic ssDNA overhang, called a sticky end, that can bind the arms of two different nanostars. The assembly of such DNA nanostar hydrogel is often described in two steps shown in Fig. 1. At high temperatures, all DNA is fully denatured with isolated ssDNA strands. Below a temperature called T_{NS} the nanostars self-assemble. At a lower temperature T_{SE} the sticky ends hybridize with one another linking neighbouring nanostars. At low temperature, we get a hydrogel network.

The phase behavior of the nanostar system depends not only on the temperature but also on the initial concentration of DNA, as shown on Fig. 1. At high enough concentration and below T_{SE} , the network of nanostars spans space, whereas at low concentrations a dense phase rich in DNA coexists with a dilute phase poor in DNA^{9–11,14,16}. It has been shown that the position of the phase

^a Institut Néel-CNRS/UGA-Grenoble INP, Grenoble, France.^b LIMMS-CNRS/Institute of Industrial Science-The University of Tokyo, Tokyo, Japan.^c LIP-CNRS/ENS Lyon, Lyon, France.^d Université Claude Bernard Lyon 1, CNRS, Institut Lumière Matière, UMR5306, F-69100, Villeurbanne, France.[†] Anthony Genot passed away on April 8th 2025.^{*} E-mail: mathieu.leocmach@univ-lyon1.fr.

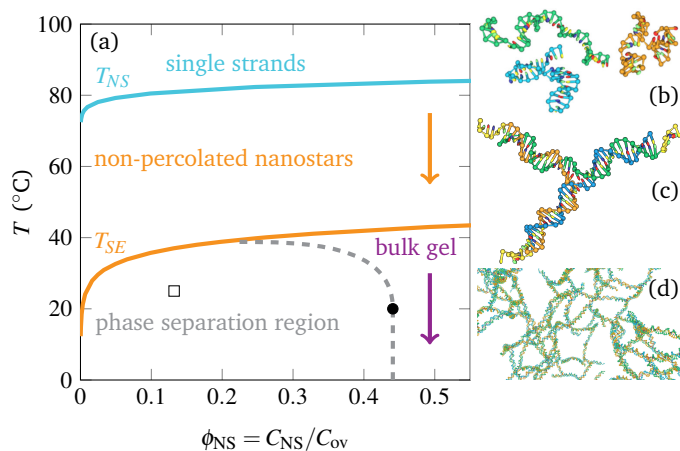


Fig. 1 (a) Theoretical phase diagram of DNA nanostars Y16SE6. The cyan and orange lines are the concentration dependence of the melting temperatures of the nanostars without sticky ends T_{NS} , respectively the duplex of sticky ends T_{SE} . The black dot is experimentally determined gel concentration at coexistence. The gray dashed line is a guide for the eye. Orange and purple arrows show concentration and the respective temperature ranges of DLS microrheology and bulk rheology measurements. (b) Snapshot of the configuration of the three isolated DNA strands at high temperature from α xDNA simulations. (c) Same for an isolated nanostar at intermediate temperature. (d) Same for a gel at the statepoint shown as an empty square in (a).

boundaries is influenced by the number of arms (valency) of the nanostars^{9,11} and the length of the sticky ends¹⁵. The phase separation pattern and kinetics are strongly altered by minute DNA sequence changes that affect the flexibility of the design¹⁷. Even though the self-assembly of the monomer motif is very precise and organized, the hydrogel network is intrinsically disordered^{10,18}. Furthermore, at high enough temperatures, the lifetime of sticky-end bonds is short^{11,12,14} and not all sticky ends are hybridized simultaneously. We thus have a disordered temperature-controlled dynamic network, the perfect test bed for a statistical physics approach to prediction of mechanical properties.

The main framework used to understand the statistical physics of DNA nanostar hydrogels is the patchy particles approach; where the nanostars are modeled as rigid particles with as many attractive patches as arms. The patches model the sticky-end interactions as they are selective, tunable, and directional. Through this modeling, the hydrogel formation is found to be similar to strong glasses^{9,11}, meaning that the timescales follow an Arrhenius trend. This relation is parametrized by the enthalpy of hybridization of the sticky ends^{11,12,14}. This results in very large variations in relaxation timescales of the material, depending on temperature. This model, together with percolation theory of limited-valence network, helped to understand the non-Newtonian response of DNA nanostar hydrogels at temperatures below T_{SE} ¹⁹. Alternatively, bulk rheological measurements below T_{SE} have been modeled using Maxwell isostaticity¹⁴. Above T_{SE} , the mechanical response of advanced DNA nanostar hydrogel designs (intermediate linker²⁰, competing strands^{13,21}) have been characterized by dynamic light scattering (DLS) microrheology, with the simplest design treated as a mere point of reference.

Indeed, above T_{SE} , the bonded sticky-ends are a minority, the network of nanostars does not span space and a simple fluid response is expected.

In this study, we will focus on the simplest DNA nanostar design and walk through the methodology of its investigation by the tools of soft matter and statistical physics. First, we will investigate its phase diagram and identify in which region the mechanical behavior is expected to be well-defined and informative. In our simple case, it means restricting our study to a large concentration regime where only continuous phases are expected. Then, we will estimate the variation of the characteristic time scale of the material depending on temperature, here a 7 orders of magnitude range. We will explain how to select complementary techniques to cover this range of time scales. In our case, we select bulk rheology and DLS microrheology and explain their respective principles. Next, we will show how a careful comparison between mechanical measurements and models can yield an understanding of nanoscale structure and dynamics. In particular, we will show that the ‘simplest DNA nanostar design’ becomes solid at much higher temperatures than expected. This hints towards a solidification mechanism that does not require percolation of the network. Finally, we will draw on the versatility of DNA technology to confront our hypothesis. We will alter the DNA nanostar design in subtle and controlled ways, measure the resulting mechanical response using the same methodology, and confirm the consistency of our model. Through this methodical exploration, we will show that DNA nanostars at high concentrations solidify in two steps upon cooling: a glass transition, followed by gelation.

2 Materials and methods

2.1 A quick tutorial about linear mechanics

At its simplest, mechanics is a study of the response of a material to a stress (force applied on an area) in terms of strain (ratio of the final size by the initial size), or the reverse. For instance, one can suddenly apply a constant stress σ and measure the resulting time-dependent strain $\gamma(t)$. The ratio $J(t) = \gamma(t)/\sigma$ is called the creep compliance. From the study of material response functions like $J(t)$, one can extract materials properties like characteristic times (in s), elastic moduli (in Pa) or viscosities (in Pa s). In turn, material properties can be related to microscopic quantities like bond lifetime or the mean distance between nodes in a network. Furthermore, the temperature dependence of material properties can be linked to thermodynamic quantities (e.g. enthalpy and entropy of binding).

All these interpretations rely on models at two levels. (i) Extracting microscopic quantities from material quantities rely on hypothesis about the microstructure, which are easier to come by and to test when the microstructure has been designed and can be altered. That is where the versatility of DNA shines. (ii) Extracting material quantities from mechanical response functions rely on mechanical models and the theory of response. For instance, a purely elastic solid can be modelled by a spring that responds to a step stress as $J(t) = 1/G$ where G is the elastic modulus. A purely viscous fluid can be modelled by a dashpot that

responds as $J(t) = t/\eta$ where η is the viscosity. Many soft materials are instead modelled by a so-called ‘spring-pot’ that responds as $J(t) = t^\alpha/\mathbb{V}$, where α is an exponent that varies between 0 (solid) and 1 (liquid) and \mathbb{V} (in Pas^α) is a quasi-property that can be considered as the modulus at $t = 1$ s if $\alpha < 0.5$ or the viscosity at $t = 1$ s if $\alpha > 0.5$ ²². Materials that have different responses depending on the time scale are modelled by a combination of springs, dashpots and spring-pots either in series or in parallel. The response functions of such models to step stress, oscillatory strain, or other mechanical stimuli can be deduced analytically (or at least numerically for more involved models), which allow fitting their parameters on experimental responses to deduce material properties.

Dynamic networks are often described by a Maxwell model, reducing the complexity of the material to a spring in series with a dashpot, quantified respectively by an elastic modulus G and a viscosity η . At time scales shorter than the characteristic time $\tau = \eta/G$ the Maxwell model behaves elastically like a solid, whereas at longer time scales it behaves like a viscous fluid.

2.2 System of study

Following¹⁵, we study mainly a 3-arm DNA nanostar (Y motif, shown in Fig. 1c), each arm composed of a 16 bp (base pairs) double-stranded segment immediately followed by a 6 bp palindromic overhang called a sticky end (SE, yellow on Fig. 1c) that is identical for each arm. The SE junction has thus little flexibility. By contrast, the junction between the arms at the center of the nanostar is flexible due to two consecutive unpaired thymine on each strand. In the following we call this design Y16SE6. We will also compare it to Y16SE0 (no sticky-end), Y16SE4 (4 bp sticky-end), Y16SE8 (8 bp sticky-end), or Y32SE6 (32 bp arms). We tuned the sequence design of the nanostar with 32 bp arms (see Table 1) so that the melting temperature is within 1 K of the nanostar with 16 bp arms. DNA sequences for the nanostars with 16 bp arms can be found in Ref¹⁵.

DNA sequences are ordered from IDT and Eurogentec in dried form, with only a desalted purification ($\sim 70\%$ purity), diluted to 5 mM, stored in 50 mM phosphate buffer 0.1 mM EDTA. For use in measuring sample properties 300 mM NaCl is added to the final solution. The concentration of each strand is $C_{\text{NS}} = 1$ mM in all measured samples, unless mentioned otherwise. For all tests, the sample is well mixed and annealed at 90 °C during at least 5 min, then the temperature is lowered at 1 °C/min to the measuring temperature.

#	Sequence 5'-3'
1	GCTAGC-ACAATACCCGGTTTGCATGGTTAAGACGTAAT-TT- TTAATATTCAGTGTATCATCCATATTCGCCAA
2	GCTAGC-TTGGCGAATATGGATGATACACTGAATATTAA-TT- GATTCAATAATGTTTCAAGGAGATAGTTGGA
3	GCTAGC-TCCAACTATCTCCTTGAAACATTATTGAAATC-TT- ATTACGTCTTAACCATGCAACCCGGTATTGT

Table 1 Sequence of the three strands of Y32SE6, each 72 bp long.

2.3 Establishing the phase diagram

Theoretical melting curve of nanostars without sticky end is obtained at any concentration C_{NS} via Nupack⁴ calculation from the sequence of the three strands of Y16SE0, each at concentration C_{NS} . We define the melting temperature of the nanostar $T_{\text{NS}}(C_{\text{NS}})$ as the temperature where half of the nanostars are assembled. In the same way, theoretical melting temperature of the SE-SE bond $T_{\text{SE}}(C_{\text{NS}})$ is determined from UNAFold²³ calculations of the assembly of the SE duplex for concentration of strands $3C_{\text{NS}}$ to take into account SE to nanostar stoichiometry. Both types of calculation are based on thermodynamic data from²⁴. The results are displayed on Fig 1 as cyan and orange curves respectively.

The coexistence concentration was determined by preparing a sample at 5 μM of each strand in a BSA-coated well, together with Evagreen for fluorescent marking. To facilitate the phase separation, the sample was incubated for 1 h with continuous 450 rpm shaking at 37 °C, a temperature just below T_{SE} , followed by centrifugation (well-plate centrifuge 3600 rpm) until all the DNA dense phase was gathered in a single droplet ($\approx 400 \mu\text{m}$ laterally) containing DNA-poor phase inclusions. Then we acquired a 3D stack of the droplet using an Olympus laser scanning confocal microscope at 20x magnification that we segment to deduce the volume of the dense phase. We derive a coexistence concentration of $(894 \pm 10) \mu\text{M}$ reported on Fig 1 as a black dot.

The theoretical molar overlap concentration between nanostars is obtained as $C_{\text{ov}} = 3 \times 10^3 / (4\pi R_{\text{eff}}^3 \mathcal{N}_A)$, where \mathcal{N}_A is the Avogadro number and R_{eff} is the effective radius of a nanostar. Consistently with¹⁸, we estimate the contour radius of a nanostar as $R = n_Y u + r$, where $n_Y = 16$ is the number of base pairs in the double-stranded segments, $u = 0.332 \text{ nm/bp}$ rise per base pair in B-DNA, and $r = 0.764 \text{ nm}$ the radius of the central flexible part of the nanostar. To convert from contour radius R to effective length R_{eff} , we have to take into account the persistence length of DNA $\ell_p \approx 50 \text{ nm}$ in our high salt condition²⁵. Following²⁶ we use the expression

$$R_{\text{eff}} = R(1 + R/\ell_p)^{-2/5} \quad (1)$$

to describe the crossover between the rigid rod regime and the self-avoiding walk. We obtain $R_{\text{eff}}(n_Y = 16) \approx 5.80 \text{ nm}$. The resulting $C_{\text{ov}} \approx 2.03 \text{ mM}$ is used to scale the concentration axis in Fig. 1.

In order to perform reliable mechanical measurements, we need continuous phases and thus to remain outside of the phase separation region. Therefore, we decided to work at a concentration of 1 mM, that is both safely above coexistence and well below overlap.

2.4 Time scale

For a dynamic network as DNA nanostar hydrogels, the expected mechanical behavior is Maxwellian¹⁴, that is solid-like at time scales much shorter than the bond lifetime, and liquid-like at much longer time scales. Measuring response functions at time scales well into both regimes is necessary to fully characterize the system.

Previous studies^{11,12,14} have found that the rearrangement

time scale of DNA nanostars follows

$$\tau = \tau_0 \exp\left(\frac{n(\Delta H - T\Delta S)}{RT}\right), \quad (2)$$

where ΔH and ΔS are the molar enthalpy and molar entropy of the SE-SE bond, $n = 2$ in the case of 3-arm nanostars, and τ_0 the timescale at $T = T_{SE}$. At our concentration, $\Delta H \approx 91.5 \text{ kJ/mol}$ and $\Delta S \approx 288 \text{ J/mol/K}$ according to UNAFold²³. We thus expect a 7 orders of magnitude ratio between timescales at 90°C and at 10°C. In order to measure both solid-like regime at the highest temperature and liquid-like regime at the lowest temperature, a 9 orders of magnitude experimental window is necessary. In practice, different techniques give access to different time windows.

2.5 Rheometer

Following Conrad *et al.*¹⁴, we characterize the low temperature mechanical response of our system using bulk oscillatory rheology. This technique consists in applying a small amplitude oscillatory shear deformation $\gamma(t) = |\gamma| \cos(\omega t)$ on a macroscopic sample (here 70 μL) and measure the resulting oscillatory shear stress $\sigma(t) = |\sigma| \cos(\omega t + \delta)$, where ω is the angular frequency and δ the loss angle. In complex notations, $\sigma = G^* \gamma$, where $G^* = |G^*| e^{i\delta} = G' + iG''$ is the complex shear modulus, which real and imaginary parts are respectively the storage modulus and the loss modulus. $\tan \delta = G''/G'$ is called the loss tangent. The frequency dependence $G^*(\omega)$ is our mechanical response function. To construct it several measurements are done at different frequencies spaced logarithmically to sample the frequency range.

The frequency range of a rheometer is limited by inertia at high frequency and by torque resolution of diverging experimental time at low frequency. In the case of our geometry (cone-plate, with a metallic cone of radius 25 mm and an angle $\alpha = 1^\circ$ truncated at 50 μm), we cannot reach beyond $\omega_{\max} = 100 \text{ rad/s}$, i.e. we are limited to time scales longer than $\approx 0.1 \text{ s}$. On the low frequency end, we are limited by the sensitivity of the rheometer. Indeed the viscous response scales as ω , thus the stress becomes very small at low frequency. In practice, our lowest frequency is $\omega_{\min} = 10^{-3} \text{ rad/s}$, where a single point of the frequency spectrum is acquired in more than 1 h.

We use a stress-controlled rheometer MCR 301e from Anton Paar with a Peltier temperature controlled bottom plate. To ensure sample thermal equilibration at the set temperatures, our maximum cooling rate is 1 K/min. The three solutions, each containing one of the DNA strands are mixed directly onto the plane of the rheometer at 20°C. After the lowering of the rotor, a ring of sunflower oil is added around the cone, and the whole is covered with a solvent trap to minimize sample dry out. The sample is brought to 90°C and then gently mixed by rotating the cone. Then it is annealed, before measuring its properties at the wanted temperature.

The resolution of bulk oscillatory rheology is limited by the resolution in torque of the rheometer, $\mathcal{T}_{\min} \approx 0.1 \mu\text{Nm}$ in our case. We obtain the torque \mathcal{T} for each point and use it to define the relative error of each quantity: $\text{Error}[G']/G' = \mathcal{T}_{\min}/\mathcal{T}$, same for the loss modulus G'' , while $\text{Error}[\tan \delta]/\tan \delta = 2\mathcal{T}_{\min}/\mathcal{T}$.

2.6 DLS microrheology

In a similar way as Fernandez-Castanon *et al.*¹³, we characterize the high temperature mechanical response of our system using dynamic light scattering (DLS) microrheology. This technique consists in measuring the spontaneous dynamics of microscopic tracer particles (PS-COOH polystyrene coated with carboxyl groups of radius $a = 255 \text{ nm}$ from Bangs Laboratories) embedded at low concentration in the sample. The inertia of such small particles can be neglected at time scales larger than 10^{-7} s ²⁷. In a simple Newtonian fluid of viscosity η_s , the motion of the particles should be diffusive, with a mean square displacement

$$\langle \Delta r^2 \rangle(\Delta t) = \frac{dk_B T \Delta t}{3\pi a \eta_s}, \quad (3)$$

where $d = 3$ is the dimension of space and k_B the Boltzmann constant. Therefore measuring $\langle \Delta r^2 \rangle(t)$ and knowing the radius a of the tracers allow the extraction of the viscosity. This Stokes-Einstein relation can be generalized to viscoelastic materials as²⁸

$$\langle \Delta r^2 \rangle(\Delta t) = \frac{dk_B T}{3\pi a} J(\Delta t), \quad (4)$$

where $J(\Delta t)$ is the same creep compliance as defined in section 2.1. Eq. (4) means that particle dynamics $\langle \Delta r^2 \rangle(\Delta t)$ is the response to thermal excitation $k_B T$.

Using a commercial nanoparticle analyzer nanoPartica SZ-100V2 from Horiba, we can measure particle dynamics between 10^{-6} s and 10^{-1} s . The DNA strand and tracer solutions are mixed inside a 70 μL quartz microcuvette (Hellma 105.251-QS.Z8,5), covered by mineral oil to prevent evaporation, and directly annealed in the temperature-controlled DLS setup. We use a holder adapter to ensure good thermal conduction. After annealing, temperature is decreased by steps of 1 K, equilibrated for 5 min, and then 5 acquisitions of 2 min each are performed. We perform 5 coolings on each sample.

Each acquisition consists in shining a 532 nm laser through the cuvette and collecting the scattered light $I(q, t)$ at a 90° angle to a photomultiplier, yielding the autocorrelation function of the scattered intensity

$$g_2(q, \Delta t) - 1 = \frac{\langle I(q, t) I(q, t + \Delta t) \rangle_t}{\langle I(q, t) \rangle_t^2}, \quad (5)$$

where $q \approx 23 \mu\text{m}^{-1}$ is the wavenumber and $\langle \dots \rangle_t$ denotes time average. To ensure that the time average is equivalent to an ensemble average (ergodic condition, see Ref^{29,30}), we keep only acquisitions where $2 - g_2(q, \Delta t_{\min}) < 10^{-2}$ and where $g_2(q, \Delta t) - 1$ actually decays to zero at long times. At each temperature the remaining acquisitions are averaged, converted to intermediate scattering function $f(q, \Delta t) = \sqrt{g_2(q, \Delta t) - 1}$ and ultimately to creep compliance as

$$J(\Delta t) = -\frac{2d\pi a}{q^2 k_B T} \log f(q, \Delta t). \quad (6)$$

We consider two sources of error on g_2 : numerical errors that are important at short times where $2 - g_2 \leq 1$, and statistics of time averaging that are important at long Δt . We set the upper bound of the former to $2 - g_2(q, \Delta t_{\min})$, whereas the latter has been estimated to $6\sqrt{\Delta t/t_{\text{avg}}}$, where $t_{\text{avg}} = 2 \text{ min}$ is the total aver-

aging time^{13,31}. The error on the intermediate scattering function is then

$$\text{Error}[f(q, \Delta t)] \approx 1 - f(q, \Delta t_{\min}) + \frac{3}{f(q, \Delta t)} \sqrt{\frac{\Delta t}{t_{\text{avg}}}}. \quad (7)$$

Errors bars on the creep compliance are then obtained by carrying explicitly $f \pm \text{Error}[f]$ through the very non linear Eq. (6). Points where relative error on J is larger than 1 are discarded.

For the ergodic condition to be satisfied, we need at least two decades of liquid-like behaviour within our time window. That sets the maximum characteristic time we can measure with our DLS apparatus to 10^{-3} s.

2.7 Methods we will not use

It is possible to perform DLS on DNA samples without tracers^{9,11,12}. In this case, the technique probes the fluctuations of the DNA molecules, e.g. the relaxation of the nanostar network. In the absence of well-defined tracers it is not possible to deduce mechanical response function, and only time scales can be deduced, neither modulus nor viscosity.

The dynamics of tracers can also be obtained from experiments under a microscope^{32,33}. The accessible time scales are then limited by the frame rate of the camera, seldom above 1000 fps. Furthermore, the spatial resolution is not as good as DLS. Obtaining displacements below 30 nm is difficult, which makes moduli larger than a few Pa impossible to measure. These techniques are thus often limited to the quantification of fluid regimes¹³.

Finally, Dynamic Wave Spectroscopy (DWS) is a variant of DLS based on the multiple scattering of the light. The ergodic condition can be satisfied much more easily in DWS, which greatly extends the capacity to probe slowly relaxing mechanical responses. DWS has been used for microrheology of DNA hydrogels²⁰ but was not accessible to us at the time of this study.

3 Results and discussion

3.1 Low temperature results

Figure 2(a-c) shows the results of the frequency sweeps conducted at different temperatures of Y16SE6 at $C_{NS} = 1$ mM. For all temperatures we observe $\tan \delta > 1$ at low frequencies, that is $G' < G''$, corresponding to a fluid-like behaviour. The loss tangent decreases with increasing frequency, reaching solid-like behaviour. Consistently, the storage modulus G' increases at low frequencies until it reaches a plateau at high frequencies; whereas the loss modulus G'' increases more sharply than G' at low frequencies then reaches a maximum before it starts decreasing at high frequencies but soon reaches a plateau.

On Figure 2(d-f) we show the same data shifted by temperature dependent factors so that they collapse on a master curve. This procedure, called ‘time-temperature superposition’ is performed in two steps. (i) The frequency axis is scaled by a time $\tau(T)$ so that $\tan \delta(\omega\tau) = 1$. The resulting collapse is shown on Figure 2(d). (ii) The modulus axis is scaled by a common factor for both G' and G'' . The resulting collapses are shown on Figure 2(e,f).

On Figure 2(d) we observe a frequency dependence of $\tan \delta$ that is more complex than the $1/\omega$ dependence expected for

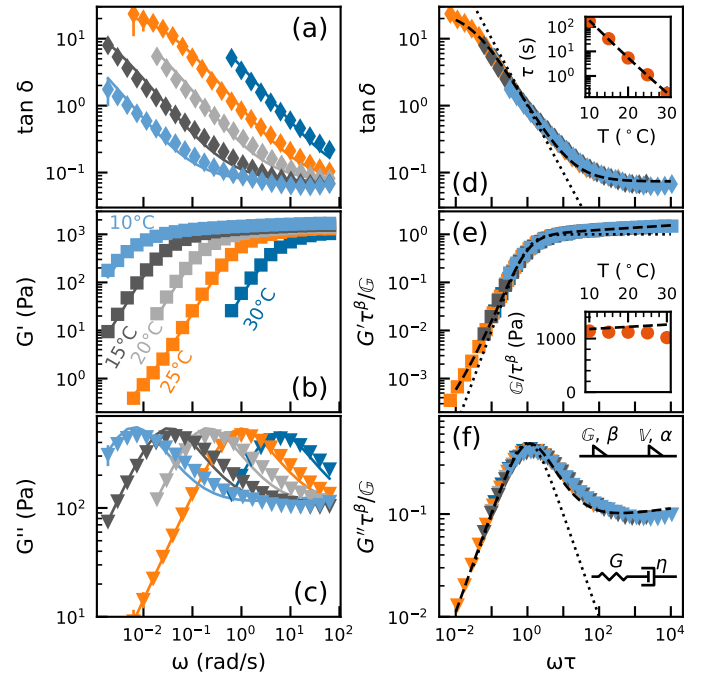


Fig. 2 Bulk rheology of Y16SE6 at 1 mM at temperatures below T_{SE} . (a) Loss factor (b) storage modulus, (c) loss modulus function of the frequency. Solid lines are fits of the fractional Maxwell model (fMM). (d-f) Time-temperature superposition of the previous. Black dashed lines show the behavior of the fMM for $\alpha = 0.98$ and $\beta = 0.05$, top diagram in (f). Black dotted lines show the behaviour of the non fractional Maxwell model, bottom diagram in (f). Insets of (d) and (e) present the temperature dependence of the fMM fit parameters, respectively the crossover characteristic timescale and the characteristic elasticity. Black dashed lines show respectively Arrhenius fit of activation energy 241 kJ/mol and modulus prediction from nanostar concentration.

a Maxwell model (dotted line). The two plateaus at low and high frequencies and the slightly decreased slope are better described by a *fractional* Maxwell model²² (dashed line). As the classical Maxwell model, the fractional Maxwell model consists in two mechanical elements in series. However these elements are spring-pots of respective exponents $\alpha > \beta$ and respective quasi-properties \mathbb{V} and \mathbb{G} . The good collapse on a single master curve indicates that $\alpha = 0.98$ and $\beta = 0.05$ can be considered constant across the temperature range. In terms of storage modulus (Fig. 2e), the difference between classical and fractional Maxwell is significant only at the extremities of the frequency range. By contrast the loss modulus (Fig. 2f) is well described only by the fractional model. The fractional description suggests a broad distribution of relaxation processes. In particular at times much shorter than the main relaxation time, when the network of SE-SE bonds can be considered permanent, relaxations already occur. Since our DNA nanostars are well-defined, the broad distribution of time scales cannot be attributed to the polydispersity of the individual components. Instead, it hints at the disordered nature of their spatial arrangements, leading to a population of possible environments, each vibrating collectively its geometry at a certain rate with no topological change.

The inset of Figure 2(d) shows the temperature dependence of τ . As expected, it follows an Arrhenius dependence compatible

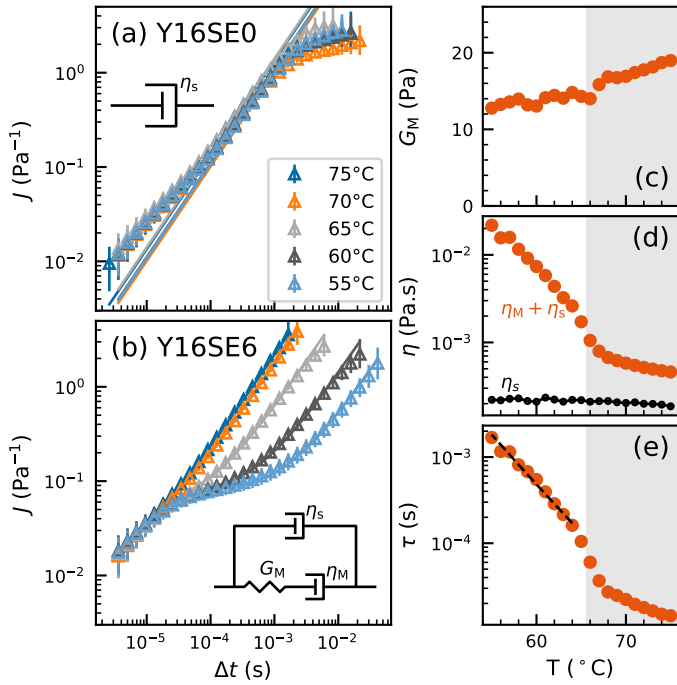


Fig. 3 DLS microrheology in Y16SE0 vs. Y16SE6 at 1 mM for temperatures above T_{SE} . (a) Compliance of nanostars without sticky ends. Solid lines are Newtonian fits. (b) Compliance of nanostars with sticky ends. Solid lines are Jeffreys model fits. (c,d,e) Temperature dependence of the parameters of Jeffreys fits of Y16SE6: (c) elasticity modulus G_M , (d) viscosity η_M and (e) characteristic time $\tau = \eta_M/G_M$. Gray area indicates the fluid temperature range where $\tan \delta > 1$ at all times. Dotted black line on (e) is an Arrhenius law of same activation energy as in the inset of Fig. 2(d).

with Eq. (2) with $n \approx 2.65$. This indicates that rearrangement involves more than the permutation of two bonds, another hint of cooperative processes. The inset of Figure 2(e) shows the temperature dependence of G/τ^β , i.e. the factor that allows the collapse of the moduli. It corresponds to the value that would have the quasi-elastic plateau at $\Delta t = \tau$. The values are compatible with the simple scaling $G = \rho_{NS} k_B T / 2$, where ρ_{NS} is the number density of nanostars¹⁹. This is consistent with the picture of a dense network where every nanostar is a cross-link that freezes in a microscopic degree of freedom.

We have seen that for $T < T_{SE}$ the mechanical behaviour of the DNA nanostar gel is better described by a fractional Maxwell model that implies collective relaxation processes, in particular in the solid-like high frequency regime. Besides this new physics, however, most of the mechanical behaviour is still understandable from the picture of a percolated network, which dynamics is governed by the lifetime of the SE-SE bond. Within this picture, no elasticity is expected above T_{SE} where the network is not percolated¹⁹.

3.2 High temperature results

Figure 3(a) shows the compliance of a suspension of nanostars without sticky-ends (Y16SE0) for several temperatures between T_{NS} and T_{SE} , obtained by DLS microrheology. All temperatures are superimposed and, in the time range where error bars are

small, the time dependence is linear. This corresponds to the behaviour of a Newtonian liquid of viscosity η that varies little in this temperature range. This is the expected behaviour in the absence of link between nanostars.

By contrast, for nanostars with sticky-ends (Y16SE6) the shape of the compliance curve evolved strongly with temperature, as shown on Figure 3(b). From a Newtonian behaviour at the highest temperature, we observe the development of a plateau at intermediate times as T is decreased. At the lowest temperature accessible to DLS microrheology, that is still ≈ 10 K above T_{SE} , the plateau spans almost 2 orders of magnitude in time. The presence of such a plateau is the unmistakable proof of an elastic regime. At shorter times, the time dependence is mostly linear with a corresponding viscosity close to the one of the buffer. After the plateau, the time dependence becomes linear again but with a much larger viscosity. Such a behaviour is also reminiscent of the behaviour of a supercooled liquid close to the glass transition³⁴.

In order to describe quantitatively these three mechanical regimes, we use the Jeffreys model, that is a viscosity η_s in parallel to a Maxwell model of modulus G_M and viscosity η_M . This model has two time scales: the entry to the plateau at $\tau_s = \eta_s/G_M$, and the exit of the plateau at $\tau = \eta_M/G_M$. Conceptually, η_s is the viscosity of the solvent (the buffer) in which nanostars are suspended, whereas G_M and η_M characterize the contribution of DNA nanostars. Here, we set aside on purpose the possibility of fractional elements in order to keep a small number of parameters. Despite this parsimony, the analytical expression of the compliance of the Jeffreys model fits well the experimental data at all accessible temperatures. The fitted modulus, shown in Fig. 3(c) is mostly constant and at least two orders of magnitude lower than the modulus measured in bulk rheology (inset of Fig 2e). Viscosities are shown in Fig 3(d). The solvent viscosity η_s remains mostly constant, following the temperature dependence of water (not shown). By contrast, the long term viscosity $\eta_M + \eta_s$ increases by two orders of magnitude in the accessible temperature range. This increase roughly mirrors the increase of the relaxation time of the network $\tau = \eta_M/G_M$ shown in Fig. 3(e). Below 65 °C, $\tau(T)$ is also well described by an Arrhenius law of same activation energy as found from bulk rheology below T_{SE} (inset of Fig 2d). We are thus confident that the dissociation of the SE-SE bonds is still setting the relaxation time of the system.

Modeling the mechanical response by the Jeffreys model allows to quantify well-defined material properties. However, even with a non zero internal modulus G_M , Jeffreys model can display a response that is mostly fluid at all time scales if τ is not much larger than τ_s . In other words, if the plateau is too short the curve $J(\Delta t)$ will not have a flat portion. Around a time scale Δt , one can approximate the compliance by a power law of exponent $\alpha = (d \log J) / (d \log \Delta t)$ ²⁸. As for the spring-pot element, $\alpha = 0$ indicates a purely elastic response at this time scale, $\alpha = 1$ a purely viscous response. More generally, the local exponent is linked to the loss tangent $\tan \delta = \tan(\frac{\pi}{2} \alpha)$. In particular $\alpha < 0.5 \Leftrightarrow \tan \delta < 1$ means that the solid response dominates at this time scale. In Figure 4(a) we display the time dependence of the loss tangent obtained from the local power law approximation of $J(t)$. We observe that for $T > 65^\circ\text{C}$ we have $\tan \delta > 1$ at all times, imply-

ing a dominant fluid response. However at lower temperatures, the material exhibits a dominantly solid response at least at some time scales. We thus confirm the emergence of elasticity some 20 K above T_{SE} .

The emergence of a short-time elasticity well above the melting temperature of the SE-SE bonds is the main result of this manuscript and cannot be explained by arguments based on percolation of the DNA nanostar network. Indeed, Nupack calculations predict that between 55 °C and 65 °C, the probability p_{SE} for a SE-SE bond to be associated ranges from 0.4 to 0.15, well below percolation threshold at $p_{SE} = 0.5$. At these values of p_{SE} , there is no percolating cluster to transmit stress. Furthermore, one can compute the probability for a nanostar to form a single bond, respectively two bonds as $P(b = 1) = 3p_{SE}(1 - p_{SE})^2$ and $P(b = 2) = 3p_{SE}^2(1 - p_{SE})$. When elasticity emerges at 65 °C, $P(b = 1) \approx 0.33$ and $P(b = 2) \approx 0.06$, meaning that most clusters of nanostars are doublets. More generally, as long as $P(b = 2) < P(b = 1)/2 \Leftrightarrow p_{SE} < 1/3$, doublets are the majority clusters and the concentration of doublets can be approximated as $C_2 \approx C_{NS}P(b = 1)/2$.

In the absence of percolation of the DNA network, we look for a different cause of elasticity: glass transition. On Figure 1, we observe that the packing fraction of nanostars is below 0.5 at our concentration, thus below usual thresholds for glass transition around 0.56-0.58. This packing fraction is computed by considering that each nanostar occupies the volume in which it is free to rotate. However, if we now consider a doublet of nanostars, its free rotation requires a volume much larger than twice the volume of an individual nanostar. Indeed, the total contour length of a doublet is $L = (4n_Y + n_{SE})u + 4r$. Its effective length L_{eff} is obtained from Eq. (1), which is linked to an effective volume allowing free rotation of a doublet $V_{rot,2} = \pi L_{eff}^3/6$. The effective volume fraction of doublets is thus $\phi_{rot,2} = V_{rot,2}C_2\mathcal{N}_A$. In our case, at $T = 65$ °C where we observe the emergence of solidity, we find that $\phi_{rot,2} \approx 0.56$, which corresponds to a usual threshold for the glass transition.

To go beyond a mere coincidence, we repeat our DLS microrheology experiments at various nanostar concentrations. We also alter the nanostar design by varying the length of the sticky ends and the length of the arms. In order to monitor systematically the emergence of solidity in these samples, we repeat the method displayed in Figure. 4(a): at each temperature we compute the loss tangent, we pick up the minimum value (orange circles) and thus obtain $\tan \delta_{min}(T)$. Solidity emerges when $\tan \delta_{min} < 1$. On Figure 4(b), we display $\tan \delta_{min}(T)$ function of the SE-SE binding probability $p_{SE}(T)$ (obtained from Nupack) for all investigated designs and concentrations. We confirm the emergence of elasticity at p_{SE} well below 1/2 for all cases, except Y16SE8 where it occurs for $p_{SE} \approx 0.42$. In any case, we observe no collapse of the data in Figure 4(b). This means that p_{SE} alone fails to describe the emergence of elasticity. We thus confirm that network percolation is not the important physical ingredient behind the emergence of elasticity in our system.

On figure 4(c), we display $\tan \delta_{min}(T)$ function of the packing fraction of freely rotating doublets $\phi_{rot,2}(T)$. Since our estimate of the concentration of doublets is correct only for small p_{SE} , the

two samples that reach $\tan \delta = 1$ for $p_{SE} > 1/3$ (Y16SE6 at 0.5 mM pale orange circles and Y16SE8 at 1 mM green circles) should be taken with a grain of salt. Indeed, they show non monotonic or decreasing trends in $\phi_{rot,2}$ with temperature, a sign that we are outside of the validity domain of our hypothesis. Once these two samples set aside, we observe two remarkable collapses of the two lengths of sticky ends (4 bp in shades of blue, 6 bp in shades of orange). The collapse of the three concentrations of Y16SE4 (blue circles) at least up to $\tan \delta_{min} = 1$, means that $\phi_{rot,2}$ captures well the concentration dependence of the emergence of elasticity. The crossing of Y16SE6 at 1 mM (orange circles) and Y32SE6 at 0.5 mM (pale orange stars) and 0.4 mM (paler orange stars) on the $\tan \delta = 1$ line despite a difference in both concentration and arm length, means that we have a good estimate of the effect of geometry in addition to the effect of concentration.

Finally, the effect that seems the less captured by our model is the length of the sticky ends, preventing a common collapse of the two families of curves. We suppose that the thermodynamics of short sticky-end assembly is not well-captured by a Nupack simulation of a sticky-end duplex. Indeed in our design without free join, the terminal base of an assembled stiky-end is neighbouring the first base of the strand of the nanostar arm, thus these two bases are able to stack together, causing additional stabilisation of the bond. This extra term should be comparatively larger for short sticky ends, pushing the Y16SE4 collapse towards larger values of $\phi_{rot,2}$. Nevertheless, our observations underline the relevance of the volume occupied by rotating doublets. When the doublets crowd each-other their rotational degrees of freedom freeze and the whole system acquire a short-time elasticity of glassy origin. At time scales longer than the life time of the SE-SE bonds, doublets are transient and a fluid behaviour is recovered.

Conclusions

We have investigated the mechanical response of a concentrated suspension of DNA nanostars of simple design, both at low temperatures by bulk oscillatory rheology, and at high temperatures by dynamic light scattering microrheology.

Below the melting temperature of the sticky-ends, we have evidenced by time-temperature superposition over 6 orders of magnitude in frequency a mechanical response well-described by a fractional Maxwell model. This description is more precise than previous ‘Maxwellian’ typology, and highlights already observed – but not interpreted – differences with the canonical Maxwell model¹⁴. In particular the fractional Maxwell model quantifies the quasi-elastic behaviour at high frequency, suggesting a broad range of relaxation times that stem from the heterogeneous disordered microstructure of the gel. We have thus demonstrated that a macroscopic mechanical test is able to quantify the disorder of the DNA assembly at the nanoscale.

Above the melting temperature, we have reported an unexpected solid behaviour at times shorter than the millisecond, responsible for a two order of magnitude increase in the viscosity felt at more usual time scales. A similar viscosity increase was reported by Fernandez-Castanon *et al.*¹³ who assigned it to the progressive formation of the viscoelastic network. Here, we have demonstrated that the emergence of solidity cannot be linked to

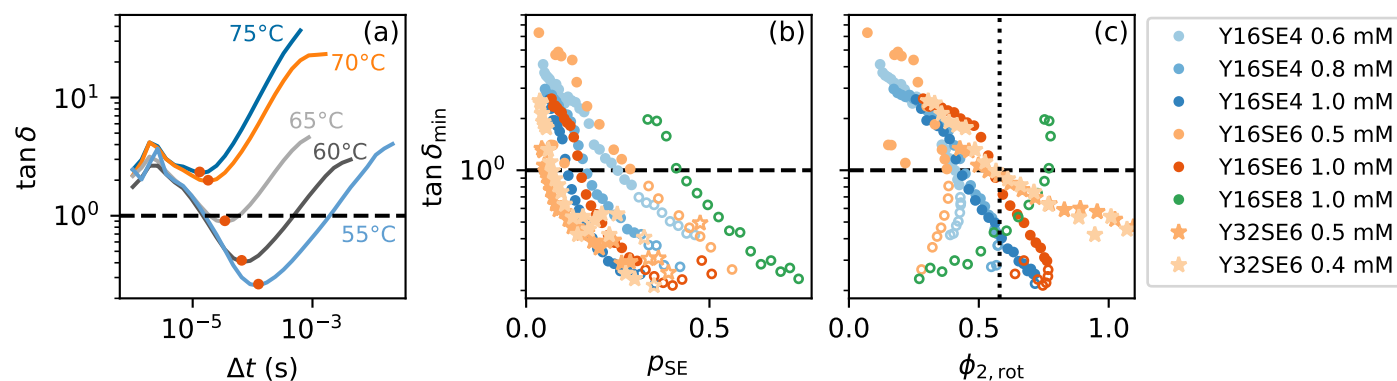


Fig. 4 Effect of sequence design and concentration on the onset of solidity. (a) For Y16SE6 at 1 mM, the loss tangent from DLS microrheology function of delay time for several temperatures. Orange circles highlight the minimum at each temperature. Below the dashed line, the behavior is solid-like. (b) For several designs, the value of the minimum of $\tan \delta$ at temperature T function of the probability of SE-SE bond at the same temperature. (c) Same as (b) but function of the volume occupied by freely rotating doublets at the same temperature. The vertical dotted line is at $\phi_{2, \text{rot}} = 0.58$. Empty symbols are for temperatures where doublets are not the majority clusters.

the percolation of the nanostar network, expected 20 K lower¹⁹. Instead, we have built a model based on the idea that the crowding of doublets of nanostars hinders their rotation, effectively locking degrees of freedom into a glass transition that induces material solidity. We have verified this model experimentally by varying the nanostar concentration and design. This model goes beyond the description of DNA nanostars as strong glass formers¹¹, and is more akin to the glass transition of dumbbells³⁵ or other anisotropic particles³⁶. We have thus shown that the solidity of DNA nanostar suspensions emerge in two steps: first a glass transition due to the crowding of rotating doublets, and second the percolation of a load-bearing DNA network.

We have also presented a methodology for mechanical investigation of DNA materials, from identifying the regions of the phase diagram where mechanical measurements are possible, to selecting measurement methods to cover the time scales, to the measurements of mechanical response functions and their modeling in terms of material properties, to hypotheses on nanoscale processes, to iterations on the design to validate the hypotheses. We hope that this method will help the nanoscale design community in embracing tools from mechanical measurement, soft matter and statistical physics to characterize and understand disordered DNA materials.

Author contributions

Investigation, including all experiments, were performed by H.A. Conceptualization and supervision by A.G., N.S., H.G., C.B. and M.L. Resources and funding acquisition provided by A.G., S.H.K., H.G., C.B. and M.L. Software provided by N.S. and M.L. Data curation, formal analysis, validation, visualisation and original draft writing by H.A. and M.L. Methodology and project administration by M.L.

Conflicts of interest

There are no conflicts to declare.

Data availability

Data for this article, including results of Nupack and UNAFold simulations, bulk rheology measurements, DLS measurements, as well as the Matplotlib³⁷ scripts to generate the figures are available at Zenodo at <https://doi.org/10.5281/zenodo.19133765>

Acknowledgements

H.A. acknowledges PhD funding from CNRS Prime program and postdoctoral funding from FY2024 JSPS Postdoctoral Fellowship for Research in Japan (short-term). H.A. and M.L. acknowledge funding from ANR ActivSoliPolar (ANR-24-CE30-6841). H.A., H.G., S.H.K. and M.L. acknowledge funding from LIMMS Internal projects. M.L. acknowledges funding from ANR VitriPSA (ANR-21-CE06-0025-02) and CNRS IRP RePAS. S.H.K. acknowledges funding from ANR DEVILISH (ANR-24-CE50-4784). H.G. acknowledges funding from CNRS MITI ElectroDSC. H.A. and M.L. thank Jan Eichler and Bruno Issenman for guidance on DDM experiments that were unfortunately not exploitable. H.A., A.G. and S.H.K. thank Kazutoshi Masuda and Miho Yanagisawa for guidance on micropipette experiments that were unfortunately not exploitable. The authors thank Luca Cipelletti for fruitful discussions and catching some of our misinterpretations of the DLS data. All remaining mistakes are ours.

This article is dedicated to the memory of Anthony Genot.

Notes and references

- 1 P. W. Rothmund, *Nature*, 2006, **440**, 297–302.
- 2 R. P. Goodman, M. Heilemann, S. Doose, C. M. Erben, A. N. Kapanidis and A. J. Turberfield, *Nature nanotechnology*, 2008, **3**, 93–96.
- 3 R. Merindol, G. Delechiave, L. Heinen, L. H. Catalani and A. Walther, *Nature communications*, 2019, **10**, 1–10.
- 4 J. N. Zadeh, C. D. Steenberg, J. S. Bois, B. R. Wolfe, M. B. Pierce, A. R. Khan, R. M. Dirks and N. A. Pierce, *Journal of Computational Chemistry*, 2011, **32**, 170–173.
- 5 N. Levy and N. Schabanel, 27th International Conference

- on DNA Computing and Molecular Programming (DNA 27), Dagstuhl, Germany, 2021, pp. 5:1–5:23.
- 6 J. Zheng, J. J. Birktoft, Y. Chen, T. Wang, R. Sha, P. E. Constantinou, S. L. Ginell, C. Mao and N. C. Seeman, *Nature*, 2009, **461**, 74–77.
 - 7 F. Li, J. Tang, J. Geng, D. Luo and D. Yang, *Progress in Polymer Science*, 2019, **98**, 101163.
 - 8 D. Wang, Y. Hu, P. Liu and D. Luo, *Accounts of Chemical Research*, 2017, **50**, 733–739.
 - 9 S. Biffi, R. Cerbino, F. Bomboi, E. M. Paraboschi, R. Asselta, F. Sciortino and T. Bellini, *Proceedings of the National Academy of Sciences*, 2013, **110**, 15633–15637.
 - 10 L. Rovigatti, F. Smallenburg, F. Romano and F. Sciortino, *ACS Nano*, 2014, **8**, 3567–3574.
 - 11 S. Biffi, R. Cerbino, G. Nava, F. Bomboi, F. Sciortino and T. Bellini, *Soft Matter*, 2015, **11**, 3132–3138.
 - 12 G. Nava, M. Rossi, S. Biffi, F. Sciortino and T. Bellini, *Physical Review Letters*, 2017, **119**, 078002.
 - 13 J. Fernandez-Castanon, S. Bianchi, F. Saglimbeni, R. D. Leonardo and F. Sciortino, *Soft Matter*, 2018, **14**, 6431–6438.
 - 14 N. Conrad, T. Kennedy, D. K. Fygenson and O. A. Saleh, *Proceedings of the National Academy of Sciences of the United States of America*, 2019, **116**, 7238–7243.
 - 15 Y. Sato, T. Sakamoto and M. Takinoue, *Science Advances*, 2020, **6**, eaba3471.
 - 16 N. Conrad, G. Chang, D. K. Fygenson and O. A. Saleh, *Journal of Chemical Physics*, 2022, **157**, 234203.
 - 17 D. T. Nguyen and O. A. Saleh, *Soft Matter*, 2017, **13**, 5421–5427.
 - 18 E. Locatelli, P. H. Handle, C. N. Likos, F. Sciortino and L. Rovigatti, *ACS Nano*, 2017, **11**, 2094–2102.
 - 19 G. Nava, T. Yang, V. Vitali, P. Minzioni, I. Cristiani, F. Bragheri, R. Osellame, L. Bethge, S. Klusmann, E. M. Paraboschi, R. Asselta and T. Bellini, *Soft Matter*, 2018, **14**, 3288–3295.
 - 20 Z. Xing, A. Caciagli, T. Cao, I. Stoev, M. Zupkauskas, T. O'Neill, T. Wenzel, R. Lamboll, D. Liu and E. Eiser, *Proceedings of the National Academy of Sciences*, 2018, **115**, 8137–8142.
 - 21 F. Bomboi, D. Caprara, J. Fernandez-Castanon and F. Sciortino, *Nanoscale*, 2019, **11**, 9691–9697.
 - 22 A. Jaishankar and G. H. McKinley, *Proceedings of the Royal Society A: Mathematical, Physical and Engineering Sciences*, 2013, **469**, 20120284.
 - 23 M. Zuker, *Nucleic Acids Research*, 2003, **31**, 3406–3415.
 - 24 J. SantaLucia, *Proceedings of the National Academy of Sciences*, 1998, **95**, 1460–1465.
 - 25 C. G. Baumann, S. B. Smith, V. A. Bloomfield and C. Bustamante, *Proceedings of the National Academy of Sciences*, 1997, **94**, 6185–6190.
 - 26 A. V. Dobrynin, R. H. Colby and M. Rubinstein, *Macromolecules*, 1995, **28**, 1859–1871.
 - 27 N. Makris, *Physical Review E*, 2020, **101**, 052139.
 - 28 T. G. Mason and D. A. Weitz, *Physical Review Letters*, 1995, **74**, 1250–1253.
 - 29 P. N. Pusey and W. Van Megen, *Physica A: Statistical Mechanics and its Applications*, 1989, **157**, 705–741.
 - 30 L. Cipolletti, R. Klein and E. Zaccarelli, *Neutrons, X-rays, and Light. Scattering Methods Applied to Soft Condensed Matter*, Elsevier, 2025, pp. 361–400.
 - 31 V. Degiorgio and J. B. Lastovka, *Physical Review A*, 1971, **4**, 2033–2050.
 - 32 T. G. Mason, K. Ganesan, J. van Zanten, D. Wirtz and S. Kuo, *Physical Review Letters*, 1997, **79**, 3282–3285.
 - 33 P. Edera, D. Bergamini, V. Trappe, F. Giavazzi and R. Cerbino, *Physical Review Materials*, 2017, **1**, 073804.
 - 34 A. Cavagna, *Physics Reports*, 2009, **476**, 51–124.
 - 35 S.-H. Chong and W. Götze, *Physical Review E*, 2002, **65**, 041503.
 - 36 R. C. Kramb and C. F. Zukoski, *Journal of Physics: Condensed Matter*, 2010, **23**, 035102.
 - 37 J. D. Hunter, *Computing in Science & Engineering*, 2007, **9**, 90–95.